Two-dimensional relativistic space charge limited current flow in the drift space

Y. L. Liu, S. H. Chen, W. S. Koh, and L. K. Ang

Citation: Physics of Plasmas (1994-present) **21**, 043101 (2014); doi: 10.1063/1.4869732
View online: http://dx.doi.org/10.1063/1.4869732
View Table of Contents: http://scitation.aip.org/content/aip/journal/pop/21/4?ver=pdfcov
Published by the AIP Publishing

Two-dimensional relativistic space charge limited current flow in the drift space

Y. L. Liu,[1] S. H. Chen,[1,a)] W. S. Koh,[2] and L. K. Ang[3]
[1]Department of Physics, National Central University, Jhongli 32001, Taiwan
[2]A*STAR Institute of High Performance Computing, Singapore 138632
[3]Engineering Product Development, Singapore University of Technology and Design, Singapore 138682

(Received 18 October 2013; accepted 17 March 2014; published online 1 April 2014)

Relativistic two-dimensional (2D) electrostatic (ES) formulations have been derived for studying the steady-state space charge limited (SCL) current flow of a finite width W in a drift space with a gap distance D. The theoretical analyses show that the 2D SCL current density in terms of the 1D SCL current density monotonically increases with D/W, and the theory recovers the 1D classical Child-Langmuir law in the drift space under the approximation of uniform charge density in the transverse direction. A 2D static model has also been constructed to study the dynamical behaviors of the current flow with current density exceeding the SCL current density, and the static theory for evaluating the transmitted current fraction and minimum potential position have been verified by using 2D ES particle-in-cell simulation. The results show the 2D SCL current density is mainly determined by the geometrical effects, but the dynamical behaviors of the current flow are mainly determined by the relativistic effect at the current density exceeding the SCL current density. © *2014 AIP Publishing LLC*. [http://dx.doi.org/10.1063/1.4869732]

I. INTRODUCTION

The dynamics of intense charged particle beams in a vacuum gap has remained an area of considerable interests in vacuum electronics,[1] pulsed power system,[2] and high power microwave sources,[3] etc. The space charge effect limits the maximum current density to be injected and propagate in space. When the injected current density exceeds the space charge limited (SCL) current density, charged particles are accumulated in a vacuum gap and lead to particle reflections and formation of a virtual cathode, the current flow thus is modulated and show an oscillatory behavior instead of a laminar flow.

The classical Child-Langmuir (CL) law[4] predicts the maximum current density that can be transported across a vacuum acceleration gap with a gap distance D and gap voltage φ_0 at the steady state. Assuming the initial kinetic energy of charged particles is much smaller than $e\varphi_0$, the classical one-dimensional (1D) SCL current density or the so-called CL law can be expressed as

$$J_{CL} = \frac{4}{9}\epsilon_0\sqrt{\frac{2e}{m}}\frac{\varphi_0^{\frac{3}{2}}}{D^2}, \tag{1}$$

where e and m are, respectively, the charge and mass of a charged particle, and ϵ_0 is the free space permittivity. The CL law has been extended by considering the geometrical and relativistic effects in the following studies. Luginsland *et al.*[5] first demonstrated the two-dimensional (2D) CL law in a diode by 2D particle-in-cell (PIC) simulation, Lau[6] then derived a consistent scaling law for the steady-state 2D current flow. Based on Lau's approach, a unified three-dimensional (3D) CL law for classical, weakly relativistic, and quantum SCL flow was derived.[7] The short-pulse (pulse-length is smaller than the gap distance) 2D CL law was also derived in classical[8,9] and weakly relativistic[10] regimes, respectively.

Besides the acceleration diode, the drift space is another important component used in vacuum electronic devices. The potential minimum induced by the space charge accumulation in the drift space limits the injected current density. The SCL current density depends on the gap distance and the initial kinetic energy of injected charged particle beam. Similar to the 1D classical CL law, the SCL current density in the drift space can be expressed as[11,12]

$$J_{DCL} = \frac{32}{9}\epsilon_0\sqrt{\frac{2e}{m}}\frac{\varphi_0^{\frac{3}{2}}}{D^2} = 8J_{CL}, \tag{2}$$

where J_{DCL} is eight times higher than the SCL current density J_{CL}, which is estimated by 1D classical CL law (Eq. (1)) under the same φ_0 and D. In Eq. (2), φ_0 is defined by the initial kinetic energy of injected particles $e\varphi_0 = \frac{1}{2}mv_0^2$, and v_0 is the initial velocity of charged particles. The 1D classical SCL current density in the drift space as described by Eq. (2) has been extended to short-pulse and relativistic regimes.[13] However, the assumption of the current saturation in a single direction was adopted in the derivation of Eq. (2). If the current flow injected into the drift space exceeds the SCL current density (where there should be no steady-state solutions), some features such as an abrupt drop in transmitted current and hysteresis when changing the injected current density[14,15] as observed in experiments could not be theoretically explained based on the original 1D model. Birdsall *et al.* relaxed the assumption of uni-directional flow in the 1D drift-space model and derived a 1D static theory to analyze the behaviors of the charge flow with the current density beyond the SCL current density.[11]

a)Electronic mail: chensh@ncu.edu.tw

W. B. Bridges is the first one to derive the 2D classical theory for the SCL current density in the drift space based on a series expansion method.[16] The theoretical formula can be expressed as the ratio of 2D current density limit [denoted as $J(2D)$] and 1D current density limit [denoted as $J(1D)$] in a drift space, i.e.,

$$\frac{J(2D)}{J(1D)} = \frac{1}{1-\exp\left(-\frac{\pi W}{2D}\right)}, \tag{3}$$

where W is the beam width and D is the gap distance of the drift space, respectively. But the validity of the theoretical analysis is still limited due to the application of the series expansion method in the derivation. Applications of the high energy charged particle beam are widely spread in cutting-edge researches, e.g., terahertz radiation[17,18] and X-ray[19] sources, electron microscopes,[20] free electron lasers,[21–24] charge-particle radiation therapy,[25] and proton therapy.[26,27] The relativistic effects of energetic charged particle beam propagating in the drift space need to be taken into account for the derivation of 2D CL law.

In Sec. II, a 2D relativistic CL law (ignoring the self-magnetic field) for the current flow in a drift space is presented. An electrostatic (ES) PIC simulation was employed to verify the 2D CL law using the over-injection method (OIM) and the potential-matching method (PMM). In Sec. III, the theoretical analysis was extended to study the dynamical behaviors of the 2D relativistic current flow at the current density beyond the SCL current density. The extended 2D theory shows how the transverse geometry and the relativistic factor affect the behaviors of the current flow, e.g., the transmitted current fraction f, the potential minimum φ_m, the minimum potential position ξ_m in the drift space, and virtual cathode oscillation frequency, by changing the current density from the values below the current density limit to few times of the current density limit. The 2D ES PIC simulation was performed to verify the static theory as well as to demonstrate virtual cathode oscillations and dynamics of the current flow under the slowly time-varying current injection. Section IV gives the summary and conclusions.

II. TWO-DIMENSIONAL SCL CURRENT DENSITY IN DRIFT SPACE

Considering a uniform injection of charged particles with initial velocity v_0 over a finite strip of width W in a planar drift space of gap distance D, the electric field in the center of injecting surface can be described by

$$E = \int_{D/2}^{D}\int_{-W/2}^{W/2} \frac{\rho(x,z)}{2\pi\epsilon_0}\frac{z}{(x^2+z^2)}dxdz, \tag{4}$$

where $\rho(x,z)$ is the charge density within the drift space and z is the direction of beam propagation. The range of the integration over z in Eq. (4) starts from $D/2$ because the charge distribution function $\rho(x,z)$ is symmetric with respect to $z = D/2$. Based on the method proposed by Lau[6] with the assumption of uniform charge distribution in transverse direction, the charge density can be assumed to be independent of x, i.e., $\rho(x,z) \sim \rho(z)$. Eq. (4) thus can be rewritten as

$$E(2D) = \frac{J(2D)}{\pi\epsilon_0}\int_{\frac{D}{2}}^{D}\frac{1}{v(z)}\tan^{-1}\left(\frac{W}{2\left(z-\frac{D}{2}\right)}\right)dz, \tag{5}$$

where $J(2D) = \rho(z)v(z) = constant$ is the injected current density. The mathematical relation $\tan^{-1}(p) = \frac{\pi}{2} - \frac{1}{p}$ at $p \gg 1$ is used for solving the integration of Eq. (5). The 1D approximation of the space charge field can be recovered by setting $W \to \infty$, i.e.,

$$E(1D) = \left(\frac{J(1D)}{2\epsilon_0}\right)\int_{D/2}^{D}\frac{dz}{v(z)}. \tag{6}$$

When the injected current density reaches the current density limit, the electric field in the center of the emitting strip is assumed to satisfy $E(2D) = E(1D)$. The 2D SCL current density for the drift space in terms of 1D limit is given by

$$\frac{J(2D)}{J(1D)} = \left\{1 - \frac{2}{\pi}\frac{\int_{D/2}^{D}\frac{1}{v(z)}tan^{-1}\left(2\frac{\left(z-\frac{D}{2}\right)}{W}\right)dz}{\int_{D/2}^{D}\frac{1}{v(z)}dz}\right\}^{-1}. \tag{7}$$

Since the charge density is assumed to be only dependent upon z, the term $z - \frac{D}{2}$ in Eq. (7) can be expressed as a function of beam velocity using the results of 1D theory,[11] i.e.,

$$z - \frac{D}{2} = \left(\frac{4\epsilon_0}{9J}\frac{\varphi_0}{v_0{}^2}\right)^{1/2}\sqrt{(v-v_m)(v+2v_m)^2}, \tag{8}$$

where $v_m = \sqrt{\frac{2e\varphi_m}{m}}$ is minimum velocity of charged particles in the center of the drift space. Therefore, the 2D classical SCL current density in a drift space can be calculated using Eqs. (7) and (8). In the 1D limit, i.e., $W \gg D$, Eq. (7) can be expressed as a simple analytical form

$$\frac{J(2D)}{J(1D)} = \frac{1}{1-\frac{7}{8\pi}\left(\frac{D}{W}\right)}. \tag{9}$$

In the relativistic regime, the energy conservation law $e\varphi_0 = \frac{1}{2}mv_0^2$ is replaced by $e\varphi_0 = (\gamma_0 - 1)mc^2$. Therefore, Eq. (8) should be rewritten as $(z - \frac{D}{2}) = (\frac{\epsilon_0 mc^3}{2eJ})^{\frac{1}{2}}\int_{\gamma_m}^{\gamma_0}(\sqrt{\gamma^2-1} - \sqrt{\gamma_m{}^2-1})^{-\frac{1}{2}}d\gamma$, where $\gamma_m = \gamma_0^{1/4}$ is the minimum value of γ factor in the drift space. Following the same processes for deriving Eq. (9), the ratio of relativistic 2D SCL current density in the drift space can be expressed as

$$\frac{J(2D)}{J(1D)} = \left\{1 - \frac{2}{\pi}\frac{\int_0^{y_0}\tan^{-1}\left(\frac{D}{W}\frac{g(y)}{g(y_0)}\right)dy}{y_0}\right\}^{-1}, \tag{10}$$

where $g(y) = \int_0^y \frac{2(y^2+1)(\gamma_m{}^2-1)^{\frac{3}{4}}}{\sqrt{(y^2+1)^2(\gamma_m{}^2-1)+1}}dy$ and $y = \sqrt{\left(\frac{\gamma^2-1}{\gamma_m{}^2-1}\right)^{1/2}-1}$.

The 2D ES PIC simulation was then performed for examining the validity of the SCL current density in the drift space derived by the theoretical analyses. In the simulation, charged particle beams with the initial beam energy $U_0(\equiv\frac{e\varphi_0}{mc^2})=0.1$ in the classical regime and $U_0=10$ in the relativistic regime, respectively, are considered to propagate in a drift space with gap distance $D=1$ cm. The beam width is varied from $W=1$ cm (2D approximation: $W/D=1$) to $W=200$ cm (1D approximation: $W/D=200$). The numerical SCL current density calculated by simulations at $W/D=200$ is taken as the reference value of 1D approximation and denoted as $J(1D)$. The criteria for determining the SCL current density in PIC simulation is always an arguable issue, especially in the drift space. However, the zero longitudinal electric field at the beam-injection end for an acceleration diode is no more a proper criteria for the current flow in a drift space because the initial kinetic energy of the charged particle beam cannot be ignored. Therefore, both the OIM and PMM were used to determine the current density limit in the PIC simulation.

The PMM is applied to determine the SCL current density in the drift space by matching the potential minimum calculated by 2D PIC simulation with the 1D theoretical result.[11] The 1D theory shows the potential minimum is equal to $\frac{\varphi_0}{4}$ in the classical regime when the injected current density reaches the current density limit. So the SCL current density can be obtained by 2D PIC simulation when the numerical potential minimum is approximately equal to $\frac{\varphi_0}{4}$ at the steady state. On the other hand, the OIM determines the SCL current density by detecting the occurrence of the reflected current flow on the surface at the beam-injection end. If the injected current density is lower than the SCL current density, the current flow can totally pass through the drift space without any reflection. The SCL current density can be obtained by gradually increasing the injected current density in a series of computer runs with the time duration of ten times of beam transit time T_0 (time for a single charged particle transiting the gap) for the system to reach the steady state.

Figure 1 shows comparisons between the theoretical results and simulation results using the two methods for determining the current density limit in the classical regime $(U_0=0.1)$ and the relativistic regime$(U_0=10)$, respectively. The simulation results using both OIM and PMM show excellent agreement with the theoretical results at $\frac{W}{D}>1$, since the steady-state charge density for these cases is uniform in the transverse direction as assumed in the theoretical model. The relative errors between the simulation results and theoretical analysis are mostly less than $\pm5\%$ within the range $\frac{W}{D}>1$, as shown in Figs. 1(c) and 1(d), respectively. Here, the relative error is defined as $\Delta[\%]\equiv\frac{J(2D)_{simulation}-J(2D)_{theory}}{J(2D)_{theory}}\times100\%$. The effect of beam expansion becomes more significant at $\frac{W}{D}\leq1$, such that outermost charged particles considerably move transversely outward from their initial positions during passing through the drift space. Therefore, the 2D SCL current density estimated by the theoretical analysis is expected to be smaller than the simulation result. The relative error between the theoretical results and simulation results could be considerably reduced by applying an external magnetic field to reduce the beam expansion in the PIC simulation, as illustrated by the star sign in Figs. 1(a) and 1(c). The beam expansion is less significant in the relativistic regime. Therefore, the simulation results agree well with the theoretical results even in the absence of an externally applied magnetic field, as shown in Figs. 1(b) and 1(d).

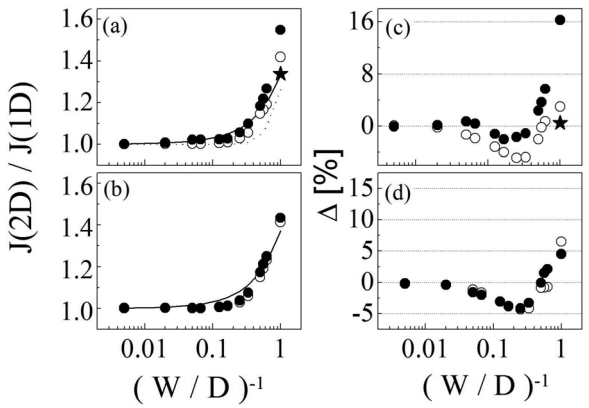

FIG. 1. Figures show the SCL current density calculated by theoretical analyses and PIC simulation in (a) classical regime and (b) relativistic regime, respectively. The corresponding errors are shown in (c) and (d) for classical regime and relativistic regime, respectively. The solid line denotes the theory derived in the study; the dashed line denotes the Bridge's theory; Symbols • denote the simulation results obtained using OIM; Symbols ○ denote the simulation results obtained using PMM; The symbols ★ in (a) and (c) denote the simulation result with an externally applied magnetic field in the PIC simulation to reduce the beam expansion.

Figure 1(a) also shows the comparisons between the theoretical results calculated by Bridge's theory[16] and the newly derived theory in the study. It is obvious that the Bridge's theory considerably deviates from the simulation results when reducing the beam width, meanwhile, the newly derived formula shows better agreement with the PIC simulation. The reason might be due to the evolution of the current flow in the simulation deviates from the specific current profile imposed by Bridge's theory while reducing the beam width. The severe imposition in Bridge's theory is relieved by taking direct integration over the charge distribution in the newly derived formulations, which shows more consistent results as compared to the simulation results. Comparisons between Figs. 1(a) and 1(b) also leads to an important conclusion, i.e., the geometrical effect dominates the current limit ratio $\frac{J(2D)}{J(1D)}$ in the drift space, while the relativistic effect plays minor role in the determination of the current limit ratio.

III. TWO-DIMENSIONAL CURRENT FLOW BEYOND CURRENT DENSITY LIMIT IN DRIFT SPACE

Considering a charged particle beam with the initial beam velocity v_0 and current density $J_{D0}(1D)$, which value exceeds the SCL current density limit, is injected into a drift space with a gap distance D. Parts of charged particles are decelerated and bunched to form a virtual cathode in the drift space. Birdsall *et al.*[11] derived a 1D classical static theory to determine the transmitted current fraction f and the normalized position $\xi_m(\equiv\frac{x_m}{D})$ of the zero potential in the drift space under the assumption of the existence of a steady state when the injected current density exceeding the threshold. Therefore, this system can be treated as a two neighboring

regions with gap distance ξ_m and$1-\xi_m$, respectively, as shown in Fig. 2.

The charged particles are injected from the upstream end of region I and reflected by the potential barrier induced by charged particle accumulation near ξ_m. Therefore, the steady-state charge density of region I can be expressed as $\rho_I = \frac{J_{D0}(1D)}{v_0} + \frac{-(1-f)J_{D0}(1D)}{-v_0}$, which is associated with the injected current density $J_{D0}(1D)$ and the reflected current density$(1-f)J_{D0}(1D)$. The charge density in region II is only associated with the current density across the potential barrier $fJ_{D0}(1D)$ (as shown in Fig. 2) in the drift space, i.e., $\rho_{II} = \frac{fJ_{D0}(1D)}{v_0}$. The integrations of Poisson's equation by eliminating ρ and v_0 with boundary conditions, i.e., $\varphi(0) = \varphi(1) = \varphi_0$ and $\varphi(\xi_m) = \varphi'(\xi_m) = 0$ for region I and region II, respectively, give the formulations for calculating the normalized potential minimum position ξ_m and transmitted current fraction$f$,[11] i.e.,

$$\alpha = 2\left[\frac{\sqrt{f(2-f)}+1}{f(2-f)}\right] \tag{11}$$

and

$$\xi_m = \frac{\sqrt{f(2-f)}-f}{2(1-f)}, \tag{12}$$

where $\alpha \equiv \frac{J_{D0}(1D)}{J_{CL}}$ is the injected current density normalized to the 1D SCL current density in an acceleration diode.

Based on Birdsall's approach, the 1D static theory, as shown in Eqs. (11) and (12), can be extended to the 2D relativistic regime by considering both relativistic and finite width effects of the charged particle beam in the drift space. The drift space is divided into two regions along the beam-propagation direction (as shown in Fig. 2) with the potential minimum equals to zero at the common boundary of these two regions when the injected current density exceeding the current density limit. It is worth noting that the system is

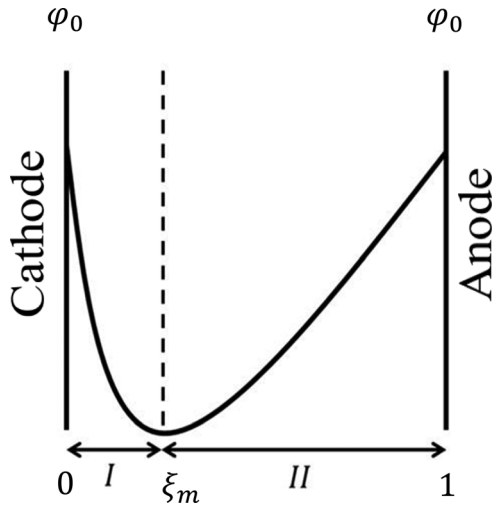

FIG. 2. The figure shows the potential profile for the injected current density exceeding the current density limit. The potential minimum equals to zero and locates at ξ_m.

equivalent to the combination of two back-to-back diodes with the zero potential at the common boundary, such that the sizes of these two diodes (or the zero potential position in the drift space) and the transmitted current fraction are determined by the SCL current density of these two diodes if the steady state of the system can be achieved. It is arguable to treat the system as the combination of two back-to-back diodes on the basis of the physical intuition, since the current flows in region I and region II are quite different. However, it turns out that a net opposite velocity profile of the electron flow in region I when the system reaches a steady state makes it possible to treat region I equivalent to a physical diode.

The 2D SCL current density in region I (with injected and reflected currents) and region II (with the transmitted current) are denoted as $\frac{J_I(2D)}{J_I(1D)} = 1 + \frac{x_m}{\pi W}$ and $\frac{J_{II}(2D)}{J_{II}(1D)} = 1 + \frac{D-x_m}{\pi W}$, which are, respectively, normalized to the corresponding 1D SCL current density.[6] According to 1D CL law, the 1D SCL current densities in the two regions can be expressed as $J_I(1D) = (\frac{D}{x_m})^2 J_{CL}(1D)$ and $J_{II}(1D) = (\frac{D}{D-x_m})^2 J_{CL}(1D)$, where $J_{CL}(1D)$ is the 1D SCL current density in a diode of gap separation D, as the described by Eq. (1). The 2D SCL current densities in two regions are, respectively, denoted as $J_I(2D) = (2-f)J_{D0}(2D)$ and $J_{II}(2D) = fJ_{D0}(2D)$, where $J_{D0}(2D)$ is the 2D injected current density in the drift space. Therefore, the relationships between $\frac{J_I(2D)}{J_I(1D)}$, $\frac{J_{II}(2D)}{J_{II}(1D)}$ and $\alpha(2D) \equiv \frac{J_{D0}(2D)}{J_{CL}(2D)}$ are expressed as

$$\begin{aligned}\frac{J_I(2D)}{J_I(1D)} &= \frac{(2-f)J_{D0}(2D)}{\left(\frac{D}{x_m}\right)^2 J_{CL}(1D)} \times \frac{J_{CL}(2D)}{J_{CL}(2D)} \\ &= \alpha(2D)\left(1+\frac{D}{\pi W}\right)\frac{(2-f)}{\left(\frac{D}{x_m}\right)^2} = 1 + \frac{x_m}{\pi W}\end{aligned} \tag{13}$$

and

$$\begin{aligned}\frac{J_{II}(2D)}{J_{II}(1D)} &= \frac{fJ_{D0}(2D)}{\left(\frac{D}{D-x_m}\right)^2 J_{CL}(1D)} \times \frac{J_{CL}(2D)}{J_{CL}(2D)} \\ &= \alpha(2D)\left(1+\frac{D}{\pi W}\right)\frac{f}{\left(\frac{D}{D-x_m}\right)^2} = 1 + \frac{D-x_m}{\pi W},\end{aligned} \tag{14}$$

where $\frac{J_{CL}(2D)}{J_{CL}(1D)} = 1 + \frac{D}{\pi W}$.[6] Rearranging Eqs. (13) and (14), the normalized minimum potential position ξ_m and transmitted current fraction f for the drift space in 2D classical regime are, respectively, expressed as

$$\begin{aligned}\alpha(2D) = \frac{1}{2\left(1+\frac{D}{\pi W}\right)}&\left\{\left(1+\frac{D}{\pi W}\xi_m\right)\left(\frac{1}{\xi_m}\right)^2\right. \\ &\left.+\left(1+\frac{D}{\pi W}(1-\xi_m)\right)\left(\frac{1}{1-\xi_m}\right)^2\right\}\end{aligned} \tag{15}$$

and

$$f = 2\left\{1 + \left(\frac{1-\xi_m}{\xi_m}\right)^2 \frac{1+\frac{D}{\pi W}\xi_m}{1+\frac{D}{\pi W}(1-\xi_m)}\right\}^{-1}, \qquad (16)$$

where $\alpha(2D) \equiv \frac{J_{D0}(2D)}{J_{CL}(2D)}$ and $J_{CL}(2D)$ is the 2D CL law in an acceleration diode.[6]

The 2D static theory can be extended to the relativistic regime using the 2D relativistic CL law,[9] such that Eqs. (15) and (16) can be rewritten as

$$\alpha(2D) = \frac{1}{2(1+GF)}\left\{(1+GF\xi_m)\left(\frac{1}{\xi_m}\right)^2 + (1+GF(1-\xi_m))\left(\frac{1}{1-\xi_m}\right)^2\right\} \qquad (17)$$

and

$$f = 2\left\{1 + \left(\frac{1-\xi_m}{\xi_m}\right)^2 \frac{1+GF\xi_m}{1+GF(1-\xi_m)}\right\}^{-1}, \qquad (18)$$

where $\alpha(2D) \equiv \frac{J_{D0}(2D)}{J_{RCL}(2D)}$, $J_{RCL}(2D)$ is the 2D relativistic CL law in an acceleration diode,[9] $G \equiv \frac{4D}{\pi W}$ is the geometry factor for a long strip emitter, and $F = F(u) = \frac{1}{4}\frac{\int_0^1 Q(w,u)dp}{Q(1,u)}$ is the mean-position factor.[9] The solutions can recover to Birdsall's 1D result (Eqs. (11) and (12)) by taking the beam width $W \to \infty$ in the classical regime.

In order to verify the 2D static theory beyond the SCL current density, the 2D ES PIC simulation was performed to study the dynamics of a charged particle beam with the triangular time-dependent current injection profile (as shown in Fig. 3) in the drift space. The rise time and the fall time of the temporal current profile are chosen to be long enough to ensure that the system can reach a quasi-steady state at any time duration under the injection of the time-varying current flow. For the convenience to compare the theoretical analyses with simulation results (as shown in Fig. 4), $\alpha(2D) \equiv \frac{J_{D0}(2D)}{J_{RCL}(2D)}$ is replaced by $\frac{J_{D0}(2D)}{J(1D)} \equiv \alpha(2D) \times \frac{J_{RCL}(2D)}{J(1D)}$, where $J(1D)$ is the 1D SCL current density in the drift space.

Figure 4 shows the variation of the minimum potential position ξ_m with the normalized current density at $\frac{W}{D} = 200$

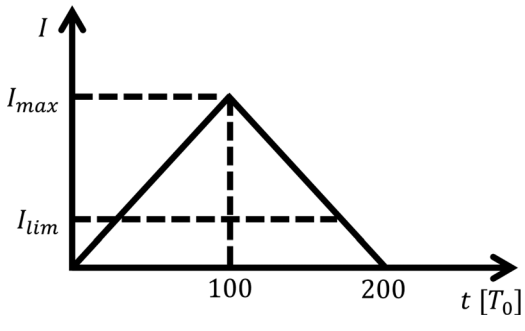

FIG. 3. The figure shows the temporal profile of the injected current density.

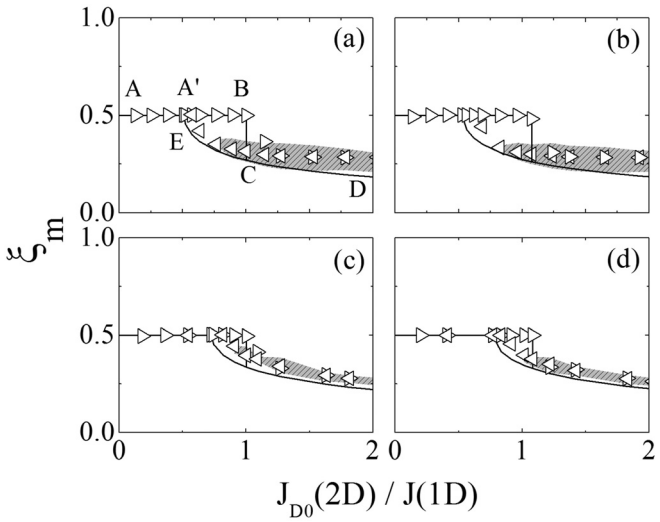

FIG. 4. Figures show hysteresis of the minimum potential position under the temporal variation of the injected current density for (a) the 1D case in classical regime ($\frac{W}{D} = 200$ and $U_0 = 0.1$), (b) the 2D case in classical regime ($\frac{W}{D} = 4$ and $U_0 = 0.1$), (c) the 1D case in relativistic regime ($\frac{W}{D} = 200$ and $U_0 = 10$), and (d) the 2D case in relativistic regime ($\frac{W}{D} = 4$ and $U_0 = 10$). The solid line denotes the theoretical results; symbols ▷ (◁) denote the averaged value under the increase (decrease) of the injected current density; the gray-slash region represents the distribution range of the values induced by the virtual cathode oscillations. The path A-B-C-D-E-A′ forms a hysteresis loop, which corresponds to the triangular time-dependent current profile shown in Fig. 3.

(1D approximation) and $\frac{W}{D} = 4$ in both classical ($U_0 = 0.1$) and relativistic regimes($U_0 = 10$), respectively. The solid lines in Fig. 4 denote the theoretical results obtained by solving Eqs. (15) and (16) for the classical regime and Eqs. (17) and (18) for the relativistic regime. The theoretical analyses show good agreement with the simulation results (triangle points). It should be pointed out that zero potential is the assumption only in theory, so the values of the potential minimum and the corresponding position calculated in the simulation, respectively, oscillate around the zero and ξ_m with time. The right-pointing triangles shown in Fig. 4 represent the simulated data during the rising of the injected current density and the left-pointing triangles represent the data corresponding to the falling of the injected current density. The theoretical zero potential position ξ_m remains at 0.5 while the injected current density is below the SCL current density (from point A to B in Fig. 4(a)), but the position abruptly drops to be less than 0.25 when the current density exceeds the current threshold (near point C) and keeps descending if the injected current density is further increased (point D). The position of potential minimum is oscillating with time due to the appearance of the virtual cathode (the gray-slash region shown in Fig. 4) from point C to point D, but its averaged value is close to the theoretical result. The position of potential minimum (denoted as left-pointing triangles) is increased along the path from point D to point E when the injected current density is decreased, which forms a hysteresis loop (A→B→C→E→A′) due to the dynamical lag between the variation of the injected current density and the system response. Therefore, the virtual cathode oscillation still exists even though the injected current density is

decreased (from point C to point E) to the level lower than SCL current density. The area enclosed by hysteresis loops of the classical cases (Figs. 4(a) and 4(b)) are quantitatively larger than that of the relativistic cases (Figs. 4(c) and 4(d)), which means that the dynamical response of the classical cases to the change in the system is much slower as compared to the relativistic cases. Figure 4 also shows that the shaded region describing the oscillation of the potential minimum is considerably narrower for the relativistic case than for the non-relativistic case, which is due to the smaller collective displacement of electrons with finite inertia responding to the oscillating field with a higher frequency (will be discussed later in Fig. 6) at the relativistic regime. Furthermore, the dynamical response to the change in the system is insensitive to the beam geometry as shown at different *W*/*D* in Fig. 4. Similar behaviors can be observed from the variations of the transmitted current fraction f induced by the time-varying injected current density in the drift space as shown in Fig. 5, in which the transmitted current factor is defined as ratio of the transmitted current diagnosed at the anode and the injected current from the cathode in simulations.

When the injected current density exceeds the SCL current density, the virtual cathode forms and oscillates near the injected region. Lin *et al.*[28] developed a computer simulation code for the studying the dynamics of the virtual cathode. The simulation results showed that the injected electron beam is modulated by the reflected electron bunch and the virtual cathode oscillation is locked to the oscillation of the reflected electron bunch. The virtual cathode oscillation frequency is found to increase with the applied voltage, but is less sensitive to the variation of the injected current density

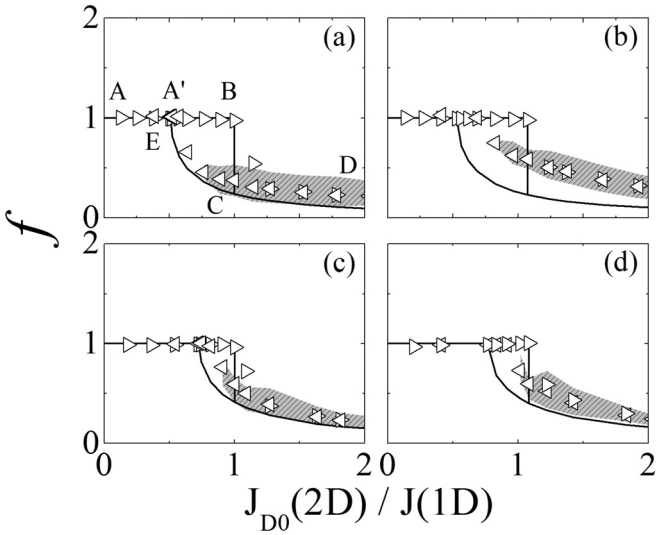

FIG. 5. Figures show hysteresis of the transmitted current fraction for (a) the 1D case in classical regime ($\frac{W}{D} = 200$ and $U_0 = 0.1$), (b) the 2D case in classical regime ($\frac{W}{D} = 4$ and $U_0 = 0.1$), (c) the 1D case in relativistic regime ($\frac{W}{D} = 200$ and $U_0 = 10$), and (d) the 2D case in relativistic regime ($\frac{W}{D} = 4$ and $U_0 = 10$). The solid line denotes the theoretical results; symbols ▷ (◁) denote the averaged value under the increase (decrease) of the injected current density; the gray-slash region represents the distribution range of the values induced by virtual cathode oscillations. The path A-B-C-D-E-A′ forms a hysteresis loop, which corresponds to the triangular time-dependent current profile shown in Fig. 3.

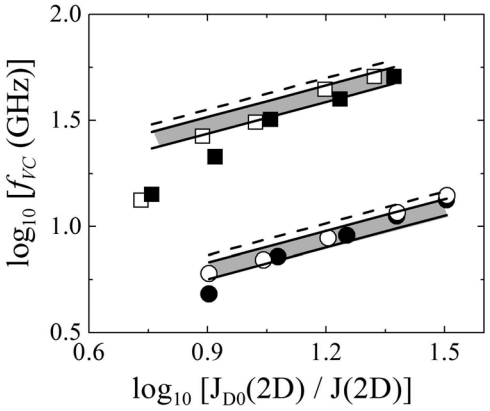

FIG. 6. The figure shows the dependencies of virtual cathode frequencies f_{VC}[GHz] on the injected current densities. Symbols • (for $\frac{W}{D} = 200$) and ○ (for $\frac{W}{D} = 4$) denote the oscillation frequencies at different injected current densities in the classical regime ($U_0 = 0.1$); Symbols ■ (for $\frac{W}{D} = 200$) and □ (for $\frac{W}{D} = 200$) denote the oscillation frequencies at different injected current densities in the relativistic regime ($U_0 = 10$). The dashed lines are calculated by Eq. (20);[30] the gray regions between two solid lines are determined by Eq. (21).[31]

and beam radius. Sze *et al.*[29] provided a theoretical formula for evaluating the oscillation frequency f_{VC} of the virtual cathode, i.e.,

$$f_{VC} = \left(\frac{4.77}{d}\right) \ln\left[\gamma_0 - \sqrt{\gamma_0^2 - 1}\right] [\text{in GHz}], \tag{19}$$

where d is the cathode-anode gap in cm and γ_0 is the relativistic factor of the injected charged particles. This formula was derived by assuming the oscillation frequency is equal to the local relativistic plasma frequency of a planar laminar flow. Fazio *et al.*[30] also proposed an empirical formula for calculating the virtual cathode oscillation frequency, which can be expressed as

$$f_{VC} = \sqrt{2\pi}\left(\frac{\omega_\perp}{2\pi}\right), \tag{20}$$

where $\omega_\perp$ is the relativistic transverse plasma frequency of the beam electrons. The formula does not explicitly show the dependency of the oscillation frequency on the geometrical factors, moreover, the validity of the formula is limited to the cases with the injected current density considerably higher than the space charge current limit. Kadish *et al.*[31] suggested that the oscillation frequency is in the range of

$$1.93 < \frac{f_{VC}}{f_p} < 2.31, \tag{21}$$

where f_p is the relativistic plasma frequency defined by the injected current density.

Fig. 6 shows the dependency of oscillation frequency f_{VC}[in GHz] of the virtual cathode on the normalized injected current density ($\frac{J_{D0}(2D)}{J(2D)}$) in both classical and relativistic regimes with the consideration of 2D geometrical effects, where $J_{D0}(2D)$ is the injected current density and $J(2D)$ is the theoretical 2D SCL current density in the drift space as

described by Eq. (10). The PIC simulation results show the consistency with Sze's theoretical results,[28] i.e., the oscillation frequency of the virtual cathode increases with the injected current density, even though the theoretical values are slightly higher than the simulation results. The simulation results are almost located within the frequency range predicted by Kadish *et al.*,[31] except few points at lower injected current density in the relativistic regime. The PIC simulation results show weak dependency on the geometrical effects, i.e., the oscillation frequencies of the virtual cathode in the 1D cases ($\frac{W}{D} = 4$) and 2D cases ($\frac{W}{D} = 200$) show little difference in both classical and relativistic regimes. But the oscillation frequencies of the virtual cathode show one order of magnitude difference when the injected beam energy is increased from $U_0 = 0.1$ to $U_0 = 10$. The examination of the dynamics of the virtual cathode provides another evidence to show that the dynamics of the current flow is mainly determined by the relativistic effect instead of the geometrical effect at the injected current density beyond the current limit.

IV. SUMMARY

The 2D ES relativistic theory for calculating SCL current density of energetic long-pulse electron flows in drift space was derived. In the regime beyond the SCL current density, the 2D relativistic static theory was derived to estimate the transmitted current fraction f and the normalized position of potential minimum ξ_m. The 2D ES PIC simulation was employed to verify the theories of SCL current density using OIM and PMM, and the largest discrepancy between simulations results and theoretical analyses is less than 7%. The 2D ES PIC simulation for the study of the current flow with the slowly time-varying current density profile demonstrates similar hysteresis phenomena with the prediction of the static theory beyond SCL current density. The virtual cathode oscillation is observed in the 2D ES PIC simulation when the injected current density exceeds the current threshold, and the oscillation frequencies show good agreement with previous theoretical analyses.

In summary, the geometrical effect of the current flow dominates the system in the regime near the SCL current density, whereas the relativistic effect dominates the dynamical behaviors of the current flow in the regime beyond the SCL current density.

ACKNOWLEDGMENTS

The work was supported by National Science Council under the Grants NSC 101-2112-M-008-012 and NSC 102-2112-M-008-013. The authors would like to acknowledge the National Center for High-Performance Computing in providing resources under the national project, "Taiwan Knowledge Innovation National Grid," and support by the National Center for Theoretical Sciences, Taiwan, ROC.

[1]J. A. Eichmeier and M. K. Thumm, *Vacuum Electronic: Components and Devices* (Springer, 2008).
[2]H. Bluhm, *Pulsed Power Systems: Principles and Applications* (Springer, 2006).
[3]A. S. Gilmour, *Microwave Tubes* (Artech House, 1986).
[4]C. D. Child, Phys. Rev. **32**, 492 (1911); I. Langmuir, *ibid.* **21**, 419 (1923).
[5]J. W. Luginsland, Y. Y. Lau, and R. M. Gilgenbach, Phys. Rev. Lett. **77**, 4668 (1996).
[6]Y. Y. Lau, Phys. Rev. Lett. **87**, 278301 (2001).
[7]W. S. Koh, L. K. Ang, and T. J. T. Kwan, Phys. Plasmas **12**, 053107 (2005).
[8]A. Valfells, D. Feldman, M. Virgo, P. G. O'Shea, and Y. Y. Lau, Phys. Plasmas **9**, 2377 (2002).
[9]W. S. Koh, L. K. Ang, and T. J. T. Kwan, Phys. Plasmas **13**, 063102 (2006).
[10]L. K. Ang and P. Zhang, Phys. Rev. Lett. **98**, 164802 (2007).
[11]C. K. Birdsall and W. B. Bridges, *Electron Dynamics of Diode Regions* (Academic, New York, 1966).
[12]R. B. Miller, *An Introduction to the Physics of Intense Charged Particle Beams* (Plenum Press, 1982).
[13]P. Zhang, W. S. Koh, L. K. Ang, and S. H. Chen, Phys. Plasmas **15**, 063105(2008).
[14]E. W. B. Gill, Philos. Mag. **49**, 993 (1925).
[15]Yu. N. Garstein and P. S. Ramesh, J. Appl. Phys. **83**, 2958 (1998); **84**, 1158 (1998); Phys. Rev. E **60**, 1069 (1999).
[16]W. B. Bridges, J. I. Frey, and C. K. Birdsall, IEEE Trans. **ED-12**, 264 (1965).
[17]C. Prokop, P. Piot, M. C. Lin, and P. Stoltz, Appl. Phys. Lett. **96**, 151502 (2010).
[18]P. Siegel, IEEE Trans. Microwave Theory Tech. **50**, 910 (2002).
[19]P. R. Ribic and G. Margaritondo, J. Phys. D: Appl. Phys. **45**, 213001 (2012).
[20]F. J. García de Abajo, Rev. Mod. Phys. **82**, 209 (2010).
[21]C. Pellegrini, Eur. Phys. J. H **37**, 659–708 (2012).
[22]B. W. J. McNeil and N. R. Thompson, Nature Photon. **4**, 814 (2010).
[23]P. Emma, R. Akre, J. Arthur, R. Bionta, C. Bostedt, J. Bozek, A. Brachmann, P. Bucksbaum, R. Coffee, F.-J. Decker, Y. Ding, D. Dowell, S. Edstrom, A. Fisher, J. Frisch, S. Gilevich, J. Hastings, G. Hays, Ph. Hering, Z. Huang, R. Iverson, H. Loos, M. Messerschmidt, A. Miahnahri, S. Moeller, H.-D. Nuhn, G. Pile, D. Ratner, J. Rzepiela, D. Schultz, T. Smith, P. Stefan, H. Tompkins, J. Turner, J. Welch, W. White, J. Wu, G. Yocky, and J. Galayda, Nature Photon. **4**, 641 (2010).
[24]T. Shintake, H. Tanaka, T. Hara, T. Tanaka, K. Togawa, M. Yabashi, Y. Otake, Y. Asano, T. Bizen, T. Fukui, S. Goto, A. Higashiya, T. Hirono, N. Hosoda, T. Inagaki, S. Inoue, M. Ishii, Y. Kim, H. Kimura, M. Kitamura, T. Kobayashi, H. Maesaka, T. Masuda, S. Matsui, T. Matsushita, X. Maréchal, M. Nagasono, H. Ohashi, T. Ohata, T. Ohshima, K. Onoe, K. Shirasawa, T. Takagi, S. Takahashi, M. Takeuchi, K. Tamasaku, R. Tanaka, Y. Tanaka, T. Tanikawa, T. Togashi, S. Wu, A. Yamashita, K. Yanagida, C. Zhang, H. Kitamura, and T. Ishikawa, Nature. Photon. **2**, 555 (2008).
[25]T. Terasawa, T. Dvorak, S. Ip, G. Raman, J. Lau, and T. A. Trikalinos, Ann. Intern. Med. **151**, 556–565 (2009).
[26]M. Goitein, A. J. Lomax, and E. S. Pedroni, Phys. Today **55**(9), 45 (2002).
[27]J. A. Efstathiou, Br. J. Cancer **108**, 1225 (2013).
[28]T. L. Lin, W. T. Chen, W. C. Liu, and Y. Hu, J. Appl. Phys. **68**, 2038 (1990).
[29]H. Sze, J. Benford, W. Woo, and B. Harteneck, Phys. Fluids **29**, 3873 (1986).
[30]M. V. Fazion, R. F. Hoeberling, and J. Kinross-Eright, J. Appl. Phys. **65**, 1321 (1989).
[31]A. Kadish, R. J. Faehl, and C. M. Snell, Phys. Fluids **29**, 4192 (1986).